AN XMM-NEWTON SURVEY FOR X-RAY EMISSION FROM GALACTIC PLANETARY NEBULAE

Nieves Ruiz[1], Martín A. Guerrero[1], You-Hua Chu[2] & Robert A. Gruenld[2]

(1)Instituto de Astrofísica de Andalucía (IAA-CSIC), (2) University of Illinois at Urbana-Champaign (UIUC)

X-RAY EMISSION FROM PLANETARY NEBULAE

Planetary Nebulae (PNe) host different sources of X-ray emission:

- Photospheric Emission: Hot, 100,000-200,000 K, central stars of PNe can emit X-rays. This emission will result in soft X-ray point sources with photon energies <0.5 keV.
- Coronal Emission from a Companion: The coronal emission from an unresolved late-type dwarf companion can produce an X-ray point source at the position of the central star. Its X-ray emission will peak at energies above 0.5 keV, in sharp contrast to the photospheric X-ray emission from a hot central star.
- Shocked Fast Stellar Wind: In the standard interacting-stellar-winds model of PN formation, the fast stellar wind emanating from the central star sweeps up the slow Asymptotic Giant Branch (AGB) wind to form a sharp nebular shell. This central cavity is expected to be filled with shock-heated fast wind that emits X-rays with a limb-brightened morphology.
- Fast Collimated Outflows: Fast collimated outflows that occur near the end of the AGB phase impinge on the AGB wind, producing bow-shock structures. When the shock velocity is >300 km s^{-1}, extended cavities filled with hot X-ray emitting gas can be formed.

The same physical agents responsible of the shaping of PNe (stellar winds, collimated outflflows, binary companions) are, thus, closely related to the production of hot gas in PNe.

XMM-NEWTON OBSERVATIONS OF PNE

PNe observations with Chandra and XMM-Newton have revealed diffuse X-ray emission associated to hot gas within the innermost nebular shells of a handful of PNe and to the fastest (≥ 500 km s-1) collimated outflows in PNe , as well as point sources at the central stars of a few PNe. These results provide information on the distribution and physical conditions of hot gas in PNe, which allow us to investigate their overall physical structure and how the energy and momentum of fast collimated outflows is transferred to the nebula.

Further progress is limited by the small number of PNe that have been detected in X-rays. A study of the evolution of X-ray emission with nebular age or among the different morphological types is not possible at this moment.

In order to build a large database of X-ray observations of PNe, we have undertaken a systematic search of the Chandra and XMM-Newton archives for pointed or serendipitous observations of PNe. In this poster, we present the results obtained using XMM-Newton observations.

The public XMM-Newton observations available by June 2007 were cross-correlated with the list of 2227 PNs and possible PNs listed in SIMBAD to search for XMM-Newton EPIC/MOS or EPIC/pn observations with an object from this list within 15´ of the aimpoint. Our search yielded 77 observations of 54 PNe or possible PNe.

The observations were retrieved from the archive for further analysis. We re-processed all observations using SAS 7.1.0 and the most up-to-date calibrations, and periods of high background were subsequently excised. The re-processed observations have been searched for X-ray emission at the location of the PNe.

RESULTS

The analysis of the XMM-Newton observations of PNe provided useful information for 44 PNe. The analysis of the observations of several PNe was not possible: RPZM 39, PM 1-265, ESO 456-55 and ESO 456-12 are located onto chip gaps; GJJC 1 and PN G353.5-05.0, in the globular clusters NGC 6656 and NGC 6441, respectively, are surrounded by bright X-ray sources; PM 1-53, PM 1-274, PM 1-2 and GRM 2 are also located on the PSF of bright X-ray sources. For all other PNe, we examined the XMM-Newton observations and determined the count rates of the sources that are detected, as well as the 3-sigma upper limits of the undetected sources. These values, together with the information on the instrument, filter, and offset from the telescope aimpoint, are listed in the following tables.
Additional work is being done to confirm the true nature of possible PNe in our sample using ground-based optical observations.

PNe DETECTED IN X-RAYS

OBJECT	INSTRUMENT	TIME_EXP (Ks)	OFFSET (′)	FILTER	COUNT RATE (cnts s^{-1})
NGC 7009	PN	22.4	1	Medium	$(47.2 \pm 1.6)\ 10^{-3}$
	MOS1+MOS2	39.4			$(10.6 \pm 0.4)\ 10^{-3}$
NGC 7026	PN	13.2	1	Medium	$(59.9 \pm 10.0)\ 10^{-4}$
	MOS1+MOS2	19.2			$(28.2 \pm 4.2)\ 10^{-4}$
NGC 7293	PN	11.4	1	Thin	$(33.9 \pm 1.8)\ 10^{-3}$
	MOS1+MOS2	15.9			$(14.3 \pm 0.7)\ 10^{-3}$
NGC 3242	PN	13.6	1	Medium	$(31.5 \pm 1.6)\ 10^{-3}$
	MOS1+MOS2	18.8			$(6.1 \pm 0.5)\ 10^{-3}$
NGC 2392	PN	10.6	1	Medium	$(39.2 \pm 2.2)\ 10^{-3}$
	MOS1+MOS2	17.5			$(8.9 \pm 0.6)\ 10^{-3}$
ESO 455-55	PN	10.8	7	Medium	$(5.1 \pm 1.1)\ 10^{-3}$
	MOS1+MOS2	31.2			$< 9.9\ 10^{-4}$
ESO 522-13	MOS1+MOS2	12.9	3	Medium	$(1.7 \pm 0.5)\ 10^{-3}$
K 1-16	PN	1.0	2	Thin	$(10.5 \pm 1.8)\ 10^{-2}$
PM 1-54	PN	45.5	5	Medium	$(44.9 \pm 4.6)\ 10^{-4}$
	MOS1+MOS2	64.5			$(14.2 \pm 2.2)\ 10^{-4}$
	PN	3.4	7	Medium	$< 3.9\ 10^{-3}$
	MOS1+MOS2	7.3			$< 12.0\ 10^{-4}$
K 3-35	PN	5.3	1	Thin	$< 2.3\ 10^{-3}$
	MOS1+MOS2	12.0			$(12.3 \pm 3.8)\ 10^{-4}$
	PN	12.2	1	Thin	$< 1.2\ 10^{-3}$
	MOS1+MOS2	16.5			$(5.2 \pm 1.8)\ 10^{-4}$
K 6-35	PN	12.0	3	Medium	$(5.5 \pm 1.4)\ 10^{-3}$
	MOS1+MOS2	30.7			$< 1.2\ 10^{-3}$
	PN	22.2	3	Medium	$< 1.7\ 10^{-3}$
	MOS1+MOS2	30.8			$< 6.2\ 10^{-4}$
ESO 456-18	PN	22.2	11	Medium	$< 2.2\ 10^{-3}$
	MOS1+MOS2	30.8			$(16.1 \pm 2.7)\ 10^{-4}$
	PN	12.0	11	Medium	$< 5.1\ 10^{-3}$
	MOS1+MOS2	30.7			$< 1.5\ 10^{-3}$
ESO 225-1	PN	5.4	1	Medium	$< 11.4\ 10^{-3}$
	MOS1+MOS2	13.5			$(2.4 \pm 0.8)\ 10^{-3}$

PNe UNDETECTED IN X-RAYS

OBJECT	INSTRUMENT	TIME_EXP (ks)	OFFSET (′)	FILTER	COUNT RATE (cnts s^{-1})
Al 2-N	PN	7.4	9	Medium	$< 2.6\ 10^{-3}$
	MOS1+MOS2	11.8			$< 10.9\ 10^{-4}$
ESO 95-8	PN	4.2	9	Medium	$< 3.4\ 10^{-3}$
	MOS1+MOS2	6.5			$< 9.6\ 10^{-4}$
ESO 133-8	PN	8.4	3	Medium	$< 20.7\ 10^{-4}$
	MOS1+MOS2	12.2			$< 6.2\ 10^{-4}$
ESO 455-37	PN	3.6	5	Medium	$< 3.7\ 10^{-3}$
	MOS1+MOS2	6.5			$< 6.2\ 10^{-4}$
ESO 456-7	PN	2.0	14	Medium	$< 2.8\ 10^{-2}$
	MOS1+MOS2	12.7			$< 3.8\ 10^{-3}$
ESO393-31	MOS1+MOS2	44.5	4	Medium	$< 1.3\ 10^{-3}$
ESO 589-6	PN	6.0	7	Medium	$< 3.3\ 10^{-3}$
	MOS1+MOS2	11.3			$< 6.8\ 10^{-4}$
ESO 456-46	PN	38.6	7	Medium	$< 1.5\ 10^{-3}$
	MOS1+MOS2	49.0			$< 5.0\ 10^{-4}$
ESO 456-50	PN	38.5	14	Medium	$< 1.5\ 10^{-3}$
	MOS1+MOS2	49.0			$< 5.4\ 10^{-4}$
ESO 456-16	PN	35.3	12	Medium	$< 19.2\ 10^{-4}$
	MOS1+MOS2	43.2			$< 7.1\ 10^{-4}$
	PN	1.8	14	Medium	$< 2.6\ 10^{-2}$
	MOS1+MOS2	12.8			$< 3.9\ 10^{-3}$
ESO 590-5	PN	2.7	6	Medium	$< 8.1\ 10^{-3}$
	MOS1+MOS2	8.6			$< 1.8\ 10^{-3}$
	PN	2.7	13	Medium	$< 11.3\ 10^{-3}$
	MOS1+MOS2	8.5			$< 1.8\ 10^{-3}$
PK 358-03 6	PN	9.2	8	Medium	$< 3.7\ 10^{-3}$
	MOS1+MOS2	23.8			$< 10.2\ 10^{-4}$
	PN	14.0	9	Medium	$< 2.7\ 10^{-3}$
	MOS1+MOS2	21.1			$< 9.5\ 10^{-4}$
PK 358-02 3	PN	7.0	9	Medium	$< 2.4\ 10^{-3}$
	MOS1+MOS2	14.1			$< 8.1\ 10^{-3}$
PK 003-03 1	PN	6.0	6	Medium	$< 5.7\ 10^{-3}$
	MOS1+MOS2	9.2			$< 1.7\ 10^{-3}$

OBJECT	INSTRUMENT	TIME_EXP (Ks)	OFFSET (′)	FILTER	COUNT RATE (cnts s^{-1})
PK 310+02 1	PN	8.7	12	Medium	$< 3.0\ 10^{-3}$
	MOS1+MOS2	14.2			$< 9.8\ 10^{-4}$
Jast 62	PN	5.9	4	Medium	$< 2.8\ 10^{-3}$
	MOS1+MOS2	10.9			$< 8.3\ 10^{-4}$
GRM 3	PN	10.6	9	Medium	$< 1.7\ 10^{-3}$
	MOS1+MOS2	23.7			$< 8.7\ 10^{-4}$
G001.1+00.0	PN	10.7	8	Medium	$< 17.7\ 10^{-4}$
	MOS1+MOS2	15.7			$< 8.3\ 10^{-4}$
	PN	26.6	11	Medium	$< 19.8\ 10^{-4}$
	MOS1+MOS2	50.1			$< 9.3\ 10^{-4}$
K 3-92	MOS1+MOS2	28.3	9	Thin	$< 8.0\ 10^{-4}$
K 5-33	PN	8.0	8	Medium	$< 3.0\ 10^{-3}$
	MOS1+MOS2	17.2			$< 9.2\ 10^{-4}$
M 3-55	MOS1+MOS2	28.6	8	Medium	$< 1.0\ 10^{-3}$
M 2-45	PN	6.8	6	Medium	$< 2.1\ 10^{-3}$
	MOS1+MOS2	19.9			$< 3.6\ 10^{-4}$
M 3-28	PN	3.8	7	Medium	$< 3.3\ 10^{-3}$
	MOS1+MOS2	7.6			$< 1.1\ 10^{-3}$
PM 2-18	PN	41.8	11	Thin	$< 0.3\ 10^{-4}$
	MOS1+MOS2	50.7			$< 3.9\ 10^{-4}$
PM 1-232	MOS1+MOS2	10.6	7	Medium	$< 10.4\ 10^{-3}$
PM 2-36	PN	4.9	3	Medium	$< 3.6\ 10^{-3}$
	MOS1+MOS2	9.6			$< 11.6\ 10^{-4}$
ShWi 5	PN	9.2	9	Medium	$< 2.8\ 10^{-3}$
	MOS1+MOS2	23.8			$< 9.5\ 10^{-4}$
SaWt 2	PN	10.4	13	Medium	$< 21.3\ 10^{-4}$
	MOS1+MOS2	14.9			$< 8.1\ 10^{-4}$
RPZM 48	PN	21.5	13	Medium	$< 13.5\ 10^{-4}$
	MOS1+MOS2	41.1			$< 7.1\ 10^{-4}$
TERZ N2022	PN	6.2	11	Medium	$< 3.3\ 10^{-2}$
	MOS1+MOS2	14.4			$< 9.6\ 10^{-4}$
WeBo 1	MOS1+MOS2	5.7	4	Medium	$< 1.3\ 10^{-3}$
	MOS1+MOS2	5.7			$< 0.4\ 10^{-3}$

Optical (left) and X-ray (right) images of NGC 3242, K 3-35 and ESO 455-37, three PNe in our survey. The optical images are over-plotted wiht X-ray contours. NGC 3242 provides a nice detection; K 3-35 is detected at ~ 3-sigma; ESO 455-37 is undetected.

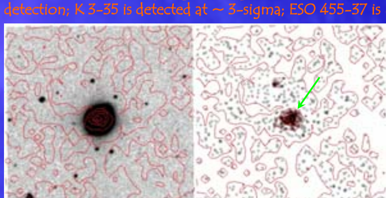

NGC 3242

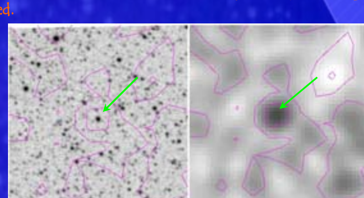

K 3-35

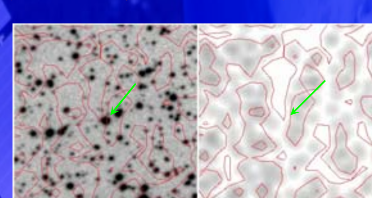

ESO 455-37

FUTURE WORK

This poster reports the first results of an on-going programme to compile X-ray observations from the most extensive sample of PNe using the Chandra and XMM-Newton archives. This database will be used to assess the occurrence of X-ray emission among PNe, searching for correlations with the evolutionary status, the nebular morphology, and the progenitor initial mass. The spatial and spectral properties of the X-ray emission will also be used to study the influence of hot gas in the nebular morphology and evolution.